AFM Observations of Phase Transitions in Molecularly Thin Films of a Three-Ring Bent-Core Compound

Yanhong Tang, Yan Wang, Xindong Wang, Shidi Xun, Chongyu Mei, Lixiang Wang, and Donghang Yan*

State Key Laboratory of Polymer Physics and Chemistry, Changchun Institute of Applied Chemistry, Chinese Academy of Sciences, Changchun 130022, People's Republic of China

Received: October 7, 2004; In Final Form: January 2, 2005

Submonolayer thin films of a three-ring bent-core (or banana-shaped) compound, *m*-bis(4-*n*-octyloxystyryl)-benzene (*m*-OSB), were vacuum-deposited on a mica surface, and a spontaneous transition from monolayer films to bilayer crystals was observed at room temperature, which was ascribed to the specific molecular shape and polar layered packing of the bent-core molecules [Tang et al. *J. Phys. Chem. B* **2004**, *108* (34), 12921−12926]. The crystal nucleation and growth from the monolayer films as well as the melting phase transition from the bilayer crystals were investigated using atomic force microscopy (AFM). It was shown that after initial nucleation, the crystal growth was achieved through three pathways: direct absorption of molecules from monolayer films, molecular cluster diffusion, and quasi-Ostwald ripening. When annealing the bilayer crystals at elevated temperatures, morphological change from a bilayer to a monolayer was observed, and some new islands with fingerlike patterns were formed during this process, which resulted from a diffusion-controlled growth of the molten molecules. In general, the high-resolution AFM in combination with the molecularly thin *m*-OSB films provided us with direct visualization of nucleation, crystal growth, melting, and film morphology evolution on the mesoscopic scale, which are of fundamental interest from the theoretical viewpoint and are of central importance for the control of interfacial properties in practical applications.

Introduction

Recently, liquid crystals composed of calamitic molecules or discotic molecules have been shown to exhibit high charge carrier mobility, anisotropic transport, and polarized emission, and they have become one of the excellent semiconductor materials for organic optoelectronic devices such as light-emitting diodes, photovoltaics, thin-film transistors, etc.[1] These properties result from the self-organization and supramolecular structures of liquid crystals, and are well-related to the molecular shape (rodlike or disk-shaped) and the phase nature (nematic, smectic, or columnar phases).[2−5] Generally, a phase with a higher order corresponds to a higher mobility, in which highly ordered, closely packed structures lead to large, ordered phase domains to facilitate intermolecular charge transport.[2,3] As a new sub-field of liquid crystals, the bent-core liquid crystals (BLCs) are attracting a great deal of synthetical and theoretical interest currently. Due to the special shape, the sterically induced pack forming lamellar structures with an in-layer polar order,[6,7] the bent-core molecules exhibit even much more attractive self-assembling properties (e.g., at least eight phases were found in them; most of them are liquid crystals and some of them show chirality and helical structures)[8,9] and peculiar physical properties (e.g., the second harmonic generation, especially the ferro- or antiferroelectricity),[10,11] indicative of potential applications in various kinds of organic molecular devices besides in liquid crystal displays.[12,13]

Organic molecular devices usually adopt a thin-film device configuration, where the vacuum-deposited methods are widely used to process low-molecular-weight materials as active layers.[14] Because the molecular-level packing strongly determines the physical properties, studies of molecular ordering, morphology, and stability of various phases at room and elevated temperatures are essential for practical applications of organic thin films.[15,16] To develop the uses for films of the unusual banana-shaped mesogens, it is necessary to understand the microstructures presented in these films and to correlate them with the extraordinary macroscopic properties. Up to now, although a considerable effort has been devoted to recognizing the bulk properties of the banana-shaped compounds, their film form has scarcely been investigated.[17,18] We have recently studied the vacuum-deposited monolayer thin films of a three-ring bent-core compound, *m*-bis(4-*n*-octyloxystyryl)benzene (*m*-OSB) (Figure 1), with atomic force microscopy (AFM) for the first time. Compared to the conventional five-ring system[19] containing sensitive Schiff-base units, *m*-OSB has a simple chemical structure and a good thermal stability up to 276 °C (indicated by thermogravimetric analysis), and it can be processed as pure thin films in high-vacuum conditions. Thus, it should be a good model compound for studying the film physics of the bent-core species. As expected, an interesting island-shape evolution with substrate temperature and a phase transition from monolayer films to bilayer crystals were observed. All these phenomena have been explained well on

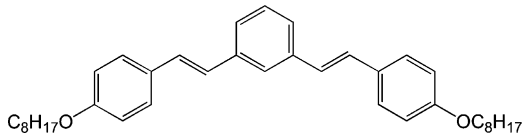

Figure 1. Chemical structure of *m*-OSB.

* Author to whom correspondence should be addressed. E-mail: yandh@ciac.jl.cn.

10.1021/jp045427x CCC: $30.25
Published on Web 03/30/2005

the basis of the specific molecular shape and characteristic layered packing of the bent-core species.[20]

This work continues the detailed studies of the thin-film phase transitions with AFM. Concerning the spontaneous phase transition from monolayer to bilayer, we attribute it to the fact that the monolayer films possess macroscopic net polarization resulting from uniform layered alignment of the dipolar bent-core molecules, and therefore they are unstable in nature.[21−23] To escape from the macroscopic polarity, the molecules will adopt a bilayer structure with the bent direction in adjacent layers antiparallel,[20] namely, an antiferroelectric alignment.[7] In conventional systems of small organic molecules or polymers, the crystallization is commonly achieved by temperature profiles, while the crystallization transition in monolayer thin films of the *m*-OSB bent-core molecule occurs at ambient temperature, making it convenient to use atomic force microscopy to follow these processes in detail, which provides direct insight into crystal nucleation, growth, as well as the surface morphological evolution.

In the present paper, we first focus on the crystallization in *m*-OSB monolayer films. Then we concentrate on the reorganization processes occurring on annealing of the bilayer crystals. We investigate the actual pathways taken by crystallization and melting with AFM real-time observations to follow changes in the films and crystals directly.

Experimental Section

The preparation of *m*-OSB thin films has been described previously, in which they were vacuum deposited on freshly cleaved mica in submonolayer coverage.[20] When the samples were stored at ambient conditions for a few days, a morphological change related to phase transition from monolayer film islands to bilayer lath-shaped crystals occurred. The film morphologies and crystallization processes were investigated using a nanoscope IIIa atomic force microscope (AFM: Digital Instruments, Santa Barbara, CA) in the tapping mode at room temperature. To check the influence of temperature on the lath-shaped crystals, samples were annealed for some time at certain temperatures according to the bulk phase sequence (i.e., the room-temperature crystal turns into another crystalline phase at 66 °C, and melts at 157 °C on heating). The annealing experiments were performed using an SPA300H/SPI3800 atomic force microscope (Seiko Instruments Industry Co., Ltd., Japan) under ultrahigh vacuum conditions. The hot-stage temperature was measured by using a small thermocouple and calibrated by indium, and the resulting morphology was in-situ imaged at the annealing temperature.

Results and Discussion

Crystallization from Monolayer to Bilayer. In the experimental substrate temperature range from RT to 120 °C, two types of islands were being observed: a dropletlike island below 40 °C and a branched island above 60 °C. Figure 2, parts a and b, shows the typical topographical images and corresponding cross sections. The height of the dropletlike islands and the branched islands is 2.5 ± 0.3 and 2.8 ± 0.3 nm, respectively, smaller than the fully stretched molecular length (∼3.6 nm), suggesting that the islands contain a single layer of *m*-OSB molecules with the long axis standing tilted relative to the interface normal (as shown in Figure 2c). When the samples were stored at ambient conditions for a few days, the films would change greatly in morphology. The monolayer islands, no matter with a dropletlike pattern or a branched pattern, would transform to crystalline grains, typically presented as in Figure 3. The lath-shaped crystals shown in Figure 3a were transited from the dropletlike islands formed at 40 °C, and those in Figure 3b were from 80 °C-deposited branched islands; no evident structural variance between them was revealed by electron diffraction. The height of the newly formed crystalline islands was 6.6−7.2 nm, corresponding to twice the molecular length. Bilayer alignment with the molecular long axis almost perpendicular to the substrate surface was consequently proposed for these lamellar crystals. The bilayer structure is shown in Figure 3c. Owing to the bent shape and particular layered packing of the bent-core molecules, the monolayer films form a macroscopic net polarization (see Figure 2c). To escape from the resulting polar order, phase transition took place and bilayer

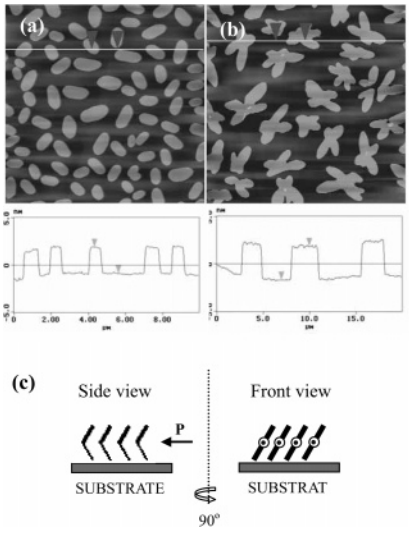

Figure 2. AFM images for *m*-OSB monolayer islands deposited on mica at the substrate temperatures of (a) RT, and (b) 60 °C; cross sections through the droplet islands and the branched islands are shown below. (c) Scheme of the monolayer structure with the molecules tilted on the surface, biaxial bent-core molecules induce a polar packing within the layer resulting in a polarization along the bent direction (P: polarization).

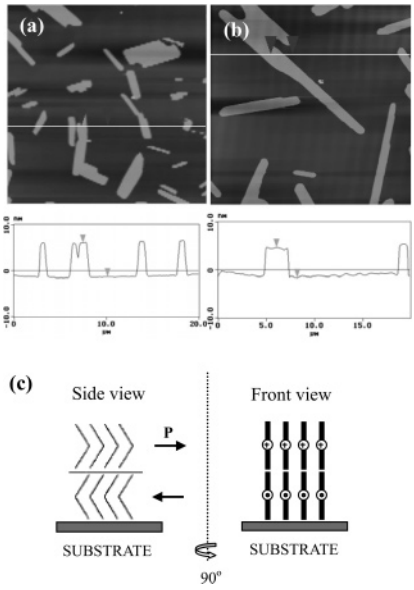

Figure 3. AFM height images and corresponding cross sections of lath-shaped crystals transited from (a) dropletlike islands deposited at 40 °C, and (b) branched islands deposited at 80 °C; (c) scheme of the bilayer structure with the molecules upright oriented on the surface, opposite alignment of the bent directivity between the layers adopted to eliminate the macroscopic polarization (P: polarization).

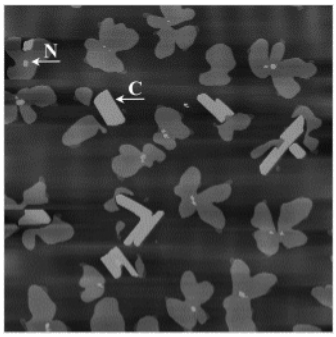

Figure 4. AFM image showing the early stage of phase transition from the branched islands. The bright dot N indicates initial nucleation within the monolayer island, and the label C indicates a growing crystal. The size of the image is 18 × 18 μm^2.

crystals with antiparallel alignment of molecules between the adjacent layers were preferred. [6,20−23]

Herein, we are interested in the phase transition of the monolayer films and investigate the detailed ordering process with atomic force microscopy (AFM). Such a high-resolution technique in combination with the geometry of a thin film of molecular thickness (two-dimensional) allows us to obtain direct information on crystal nucleation, growth, ordering, and growth patterns.[24,25] It showed that the crystallization proceeded by a two-step process beginning with the formation of nuclei and followed by the growth of ordered molecular domains around those nuclei. A representative image describing such a process is shown in Figure 4, displaying the early stage of crystalline ordering transition from the branched islands. Here, nuclei are small molecular aggregates that first appear as bright dots protruding from the monolayer (see, for example, the dot "N" in Figure 4). The phase transition is not synchronous for all the monolayer islands. In this picture, some islands just show the onset of nucleation, while others have already collapsed by the growth of the crystalline nuclei within them (for example, the crystal "C" in Figure 4). A branched island does not always correspond to a crystal, and sometimes two or more crystals are formed from a common monolayer island, depending on the number of the nucleation sites on this island (Figure 4). More commonly, a crystal grows at the expense of several monolayer islands. By measuring the size of the nuclei in the vertical direction, we know the molecules contained in these nuclei ("bright dots") are already ordered and upright oriented, and they absorb molecules from the monolayer films for direct growth into larger crystallites.

To determine detailed processes of the phase transition, we followed their growth in real-time by atomic force microscopy. Figure 5 lists four sequential images showing the time evolution of the crystals and the films. The original monolayer film was grown at the substrate temperature of 60 °C and stored at ambient conditions for about 15 days. As revealed by AFM, crystalline grains resulting from phase transition are interspersed among the branched monolayer islands. The growth fronts of a crystal labeled by circles are in contact with the monolayer films, and its growth is achieved through direct absorption of molecules from these films. The time interval between the scans is of the order of minutes, indicating a fast phase transition in such a way. Once a depletion zone is created around the crystal, the growth would stop, otherwise proceed through a different growth mechanism. As shown in Figure 5, parts a−d, the growth of the boxed crystal is not pronounced during this process, while careful inspection reveals that its neighboring monolayer island is becoming more and more slender, indicating the crystal is still growing but with a very slow rate. Figure 6, parts a and b,

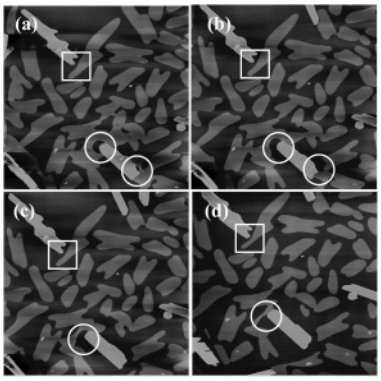

Figure 5. A series of 20 × 20 μm^2 AFM images showing how the crystallization front travels across the monolayer films: (a) $t = t_0$, (b) $t = t_0 + 42$ min, (c) $t = t_0 + 72$ min, and (d) $t = t_0 + 120$ min. The circled crystal grows larger by direct absorption of molecules from the monolayer films, and the boxed crystal grows through a different mechanism.

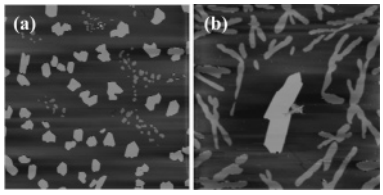

Figure 6. AFM images showing the formation of the lath-shaped crystals from (a) dropletlike islands, and (b) branched islands; no direct mass transport from the monolayer islands to the bilayer crystals was observed, indicating a quasi-Ostwald ripening mechanism. The size of the images is 30 × 30 μm^2.

shows the crystal growth by the same mechanism. In both images, the monolayer islands near the growing crystallites are small and fragmentary relative to those far away. Obviously the crystals first grew larger by directly incorporating the molecules from contiguous monolayers till the area around them was vacant, and then the crystals grew through another pathway. In this way no direct mass transport from the monolayer islands to the bilayer crystals is observed, with the growth phenomenon similar to Ostwald ripening.[26,27] The difference between them is that Ostwald ripening refers to crystal growth at the expense of other crystals of the same composition and structure. Herein, the bilayer crystals are formed at the expense of monolayer films of a different phase; however, the driving force for both cases is the elimination of unstable interfaces.

Except for the two growth modes mentioned above, we found a third growth mechanism in which crystals grew by capture of small molecular clusters separated out from the monolayer film islands. A series of typical images are shown in Figure 7, where the original dropletlike islands were formed at the substrate temperature of 40 °C and stored at room temperature for about 11 days; as a result, a large fraction of dropletlike islands have transformed into bilayer lath-shaped crystals. Figure 7a exhibits their coexistence, where none of the edges of the crystals are in contact with the monolayer islands. Many small molecular clusters with the diameter estimated to be 250−300 nm are observed at the top right corner of this picture, which are considered coming from the dropletlike islands and are migrating toward the nearby crystallites and finally adsorbed at the edges of the crystals (indicated by the circle). Figure 7b was imaged in 2 h after Figure 7a, the number of the clusters obviously increasing with time. In Figure 7c, recorded in 126 h after Figure 7a, most of the monolayer islands disappeared, and the number of the small clusters decreased due to the

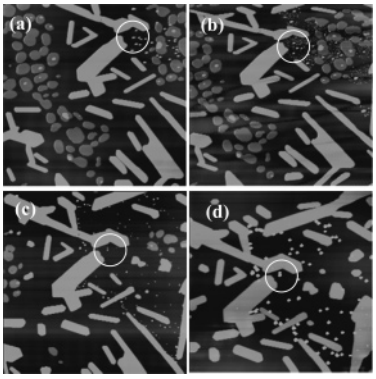

Figure 7. AFM images ($20 \times 20\ \mu m^2$) acquired at (a) t_0, (b) $t_0 + 2$ h, (c) $t_0 + 126$ h, and (d) $t_0 + 344$ h. The circles help the reader to identify the same spots on the surface showing the crystal growth by capturing the migrating molecular clusters separated out from the monolayer islands.

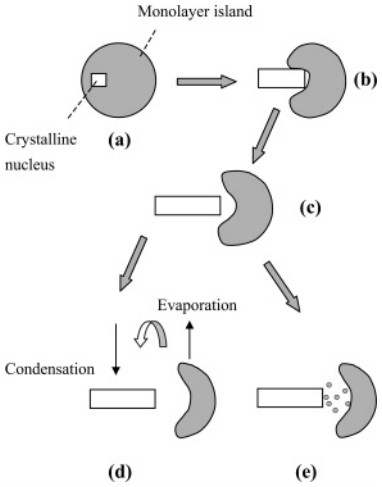

Figure 8. Scheme of the transition from monolayer to crystal: (a) formation of crystalline nucleus in a monolayer island, (b) crystal growth through direct absorption of molecules from a monolayer island, (c) a depletion zone being created around the crystal, (d) crystal growth via quasi-Ostwald ripening (evaporation−condensation model), and (e) crystal growth via molecular cluster diffusion.

absorption by the growing crystals; furthermore, their diffusional distances increased. At the final stage as shown in Figure 7d, which was recorded in 344 h after 7a, the monolayer islands were entirely consumed through the conversion into small molecular clusters, and these small clusters further coalesced to form larger molecular aggregates with the diameter up to 400−450 nm; they then migrated over a certain distance and were incorporated into the crystals at the edges. Such a cluster diffusion mechanism was also found in crystal growth from branched islands.

In summary, for the crystallization of *m*-OSB monolayer films, three growth mechanisms were revealed: direct absorption of molecules from monolayer films, migration of small molecular clusters, and quasi-Ostwald ripening. The different pathways are summarized in Figure 8. The transition velocity depends on the transport mechanisms. To a certain monolayer film, at least two mechanisms were involved in the phase transition, so it often took a long period of weeks to months from the onset of nucleation to the end of crystal growth.

Despite the same mechanisms of the phase transition and the same structure of the lath-shaped crystals for the dropletlike islands and the branched islands, there is a discrepancy in the appearance between the lath-shaped crystals from the dropletlike

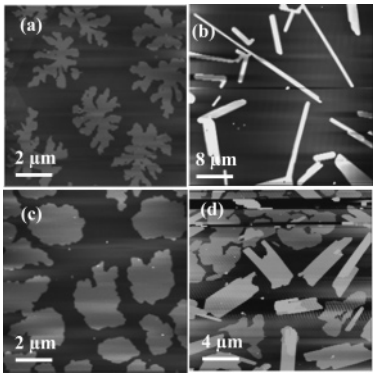

Figure 9. AFM images of phase transitions on different substrates. (a) Islands deposited on mica at 100 °C; (b) lath-shaped crystals formed from (a); (c) islands deposited on carbon-covered mica at 100 °C; and (d) lath-shaped crystals formed from (c).

islands and those from the branched islands. Due to the smaller density and larger size of the branched islands than those of the dropletlike ones, the longer diffusional distances and the anisotropic transport of *m*-OSB molecules on the surface result in crystals larger in size and aspect ratio, as shown in Figure 3b compared with Figure 3a. The unequal migrating distances of molecules cause anisotropic growth of the crystallites. The shorter distance between an edge of a crystal and the migrating molecules means the higher growth velocity of the edge, and the edge having a higher propagation velocity will become shorter,[28] typically demonstrated by the growing crystals in Figures 4 and 5. From Figures 3 and 6, we can see that the aspect ratio of the lath-shaped crystals transited from the dropletlike islands is smaller than those from the branched islands; moreover, the former have a more uniform size. We explain that, for dropletlike islands, admolecules diffuse for a relatively short distance on the substrate before being incorporated into growing crystals because of the high density (see Figure 2), hence having an increasing probability of meeting the long sides of crystals as opposed to the case of branched islands, so that the growth velocity for all the sides of crystals transformed from the dropletlike islands does not differ greatly. To further evaluate the influence of molecular diffusion on the shape and size of the crystallites, we deposited the submonolayer thin films on mica and on carbon-covered mica, respectively. Figure 9, parts a and c, shows their respective topographical image obtained at the same substrate temperature of 100 °C. As expected, both take on branched patterns, but with different island shapes and sizes. On the carbon substrate, the density of the islands is higher compared to that on the mica, and the shape of the islands on carbon is more compact. When stored at room temperature for 20 days, the branched islands on mica have completely transformed with great difference in size and aspect ratio from crystal to crystal (Figure 9b). The aspect ratios are estimated to be from 3 to 27. However, there are still some branched islands unchanged on the carbon film even after 30 days (Figure 9d), suggesting a slow phase transition in contrast with the islands on the mica substrate. The crystals on the carbon substrate show a relatively uniform size and small aspect ratios from 2 to 5. All these phenomena can again be understood by molecular diffusion. Since the growth of the branched islands is diffusion-controlled,[20] a smooth mica surface is favorable to molecular diffusion, while the rough surface of the carbon film reduces the mobility of the *m*-OSB molecules and consequently leads to an increasing nucleation. So, it should be expected on the basis of the aforementioned analysis that the crystals on carbon have a more uniform size and smaller aspect ratios than

those on mica. At the same time, the reduced diffusion of molecules on the carbon surface makes the molecule adsorbed on the island have a longer time to relax locally along the island edge before it is stuck by a new molecule, thereby yielding islands with a relatively compact shape. The rough carbon surface also lowers mass transport from the monolayer films to the bilayer crystals, giving rise to a slow phase transition. From this experiment, we can see the essential features of the island shape and the crystallization transition from monolayer to bilayer were reproduced on different substrates. It suggests that the substrate has a minor effect on the film morphology and the phase behavior, and there is a stronger interaction between the adsorbed molecules than that between the molecules and the substrate, as expected from sterically induced tight packing of the bent-core molecules.

Usually, the process of self-assembly in two-dimensions has been employed to study general aspects of crystallization and phase transitions. Molecules or particles confined to a single monolayer have fewer degrees of freedom than in three dimensions, making experimental analysis and theoretical modeling simpler.[29] Here, the crystallization transition in vacuum-deposited monolayer thin films of the *m*-OSB bent-core molecules occurs at ambient temperature and with slow rates, allowing us to distinguish clearly the two basic processes involved in the formation of crystals: nucleation (where and how the crystals start to form) and growth (how fast and under which mechanisms the crystals form) by using the AFM method. This allows for a comprehensive understanding of kinetic pathways to the crystallization in two-dimensional films. On the other hand, the first monolayer acts as a template for further film growth, and the morphology and phase behavior of the first layer have a significant influence on the growth mode of the second and subsequent layers. Several recent works revealed that charge transport in field-effect transistors is confined within the initial few organic monolayers.[30−32] The detailed investigations of the single monolayer on the microscopic scale therefore can help us understand the basic physical principles that govern organic thin-film growth, which will provide guidance for the further development and optimization of molecular thin-film devices. In our case, during the crystallization transition of the branched islands revealed by Figure 5, the monolayer films marked by the circles display a liquidlike behavior that the points with high curvature first retract, though we have confirmed that the films grown at the substrate temperature of above 60 °C are crystalline. This discovery proves useful for understanding the specific growth phenomena of the *m*-OSB thick film (to be reported in a forthcoming paper). By combining the orientational properties with the fluidity, we can obtain large-area ordered films with fewer boundaries, which are desired for high-performance organic thin-film devices.

Melting from Bilayer to Monolayer. In addition to the crystallization phase transition at room temperature, we are also interested in what will happen if we anneal the bilayer crystals at elevated temperatures? When and how do the two-dimensional *m*-OSB crystals melt? In Figure 10 we show some AFM images measured directly by an AFM of SPI 3800 at the annealing temperatures. Here we used a sample consisting of bilayer crystals of m-OSB coexisting with their monolayer dropletlike islands. Contrary to the phase transition from monolayer to bilayer at room temperature, the bilayer crystals transform into monolayer at elevated temperatures. Figure 10a shows no significant morphological changes in the crystals and films after being annealed at 60 °C for 3.5 h. When heated to 90 °C and annealed for 0.5 h, melting occurred and it first took

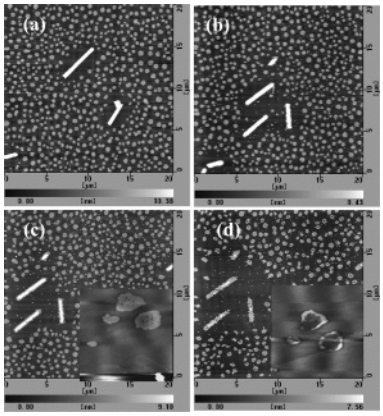

Figure 10. The morphological evolution with increased temperature imaged in situ by AFM. The sample was annealed at (a) 60 °C/3.5 h, (b) 90 °C/0.5 h, (c) 90 °C/1.0 h, and (d) 100 °C/1.0 h. The size of the images is 20 × 20 μm^2. Insets in (c) and (d) are close-ups of the dropletlike islands in them, respectively, with the size of 4 × 4 μm^2.

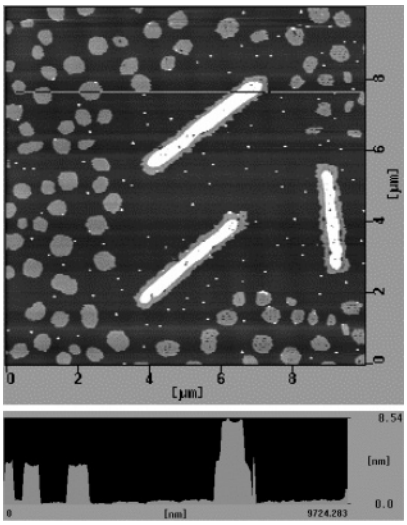

Figure 11. A magnification of a 10 × 10 μm^2 section of Figure 10c and corresponding sectional view along the line in it, showing the melting perimeter of the crystals having a height comparable to that of the dropletlike islands.

place at the periphery of the crystals and set in at the top molecular layer. At the same time, small molecular clusters of about 200 nm in diameter were found to detach from the melting lamellar crystals and the dropletlike islands (Figure 10b). On longer time scales, melting at the edges progressed into the inner of the crystalline domains (Figure 10c) and holes developed in the dropletlike islands due to the persistent detachment of the molten molecules from these islands (see the inset in Figure 10c). From the color contrast and the cross-sectional analysis shown in Figure 11, we can know the melting perimeters of the bilayer crystals have a height comparable to the original dropletlike island that contains a single layer of *m*-OSB molecules. When the temperature was raised to 100 °C for 1 h (Figure 10d), nearly all the molecules in the top layer of the original lath-shaped crystals were removed except for a small fraction of the molecules in the inner part, leaving long monolamellae behind. Simultaneously, the number of the small clusters increased and the holes in the dropletlike islands widened (see the inset in Figure 10d). It is seen that after the phase transition from bilayer crystals to monolayer films, the shape and covered area of the lamellae are roughly retained, with all the molecules in the top layer and some molecules in the bottom layer melting and diffusing away, so that holes are

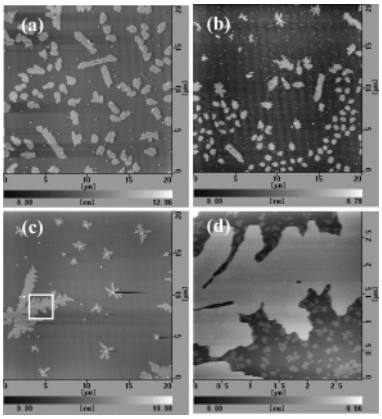

Figure 12. The same sample as in Figure 10 further annealed at the temperature of 110 °C for 0.5 h. (a), (b), and (c) were typical AFM images scanned at three different regions, and (d) a zoomed-in image of the boxed region in (c).

also observed in the monolamellae (Figure 10d). Further annealing at 110 °C for 0.5 h led to a complete phase transition (Figure 12a). In addition to the lamellar islands and the original dropletlike islands, one found some new islands with fingerlike patterns present in Figure 12, parts b and c, which were imaged at different locations on the same surface. Usually these islands are found to form at large depletion zones. Figure 12d is a zoomed-in image of the part indicated by a small square in Figure 12c, and a large number of small molecular clusters of about 100 nm in size are resolved around the branch, indicating the occurrence of molecular diffusion.

The original dropletlike islands have a uniform density on the substrate surface. After phase transition, the lath-shaped crystals adopted a bilayer structure; as a consequence, they covered less surface area, and depletion zones around the crystals were created. During annealing, as the lath-shaped crystals melted to monolayer lamellae, numerous molten molecules were detached and diffused freely on the surface. The film islands and the free molecules were not in a thermal equilibrium, and on annealing at 110 °C for some time the free molecules would attach to the islands for growth again. Some of them were adsorbed on the remainders of the lamellar islands and the dropletlike islands by migrating a short distance, while the molecules at a wide depleted zone have to be transported over a long distance before reaching an existing island. When the island distance was beyond the diffusion length of the *m*-OSB molecules, they collided with one another and aggregated to form critical nuclei,[33,34] and then served as new centers for further island growth. The island growth was diffusion-controlled and this diffusion event was revealed by Figure 12d. Different from the "hit-and-stick" model of standard DLA fractal growth,[35,36] the molecules adsorbed on the growing islands are not fixed but attempt to relax locally along the island edge (activated by thermal energy supplied by the 110 °C substrate), leading to the dendritic-like islands.[37−39] Irregular edges were also formed at the long lamellar islands and the original circular dropletlike islands due to the detachment and reattachment of molecules during this process (see, for example, Figure 12a).

We have previously reported that the dropletlike island (formed below 40 °C) had a liquid crystal-like structure and that the branched island (formed above 60 °C) was crystalline, which were indicated by the AFM morphology evolution and electron diffraction measurements.[20] Here, the partial melting of the bilayer crystals and the monolayer films followed by the molecular reorganization among the lamellar islands, the original dropletlike islands, and the newly formed fingerlike islands would lead to a homologous structure for them over long time scales. The fingerlike islands formed during the annealing process have patterns resembling those of branched islands directly grown at the mica substrate of the same temperature. It seems reasonable to consider that they have an analogous structure because of the similar nucleation and growth processes controlled by diffusion. Similarly, though the dropletlike islands maintain the elementary shape after annealing, their structure will not be liquid crystal-like anymore, but crystalline as the branched islands due to the molecular rearrangement. Nevertheless, detailed structural changes have not been investigated in this paper.

The AFM observations on the annealing of the bilamellar *m*-OSB crystal indicate that at least two steps were involved in its melting. In the first stage, the bilayer crystals melt into a monolayer structure at about 90 °C. During this process, the dropletlike monolayer islands were thermodynamically driven from an imperfect, metastable liquid crystal-like structure toward a state of higher degrees of order. Further melting experiments from the monolayer structure to a liquid occurring at a higher temperature have not been performed on them in this work. This thermodynamic behavior of the two-dimensional bilayer crystal is reminiscent of that of the *m*-OSB bulk, where the room-temperature crystal (phase I) turns into another crystalline phase (phase II) at 66 °C, and melts into an isotropic liquid at 157 °C on heating. We have already confirmed that the bilayer crystal has the same structure as that of phase I,[20] and here the films at the high-temperature substrate may be correlated with phase II.

Conclusions

Time-resolved AFM observations of phase transitions in the molecularly thin films of a three-ring bent-core compound *m*-OSB have been performed. It provides a high resolution to observe the kinetic pathways by which molecules form a crystalline state or by which order in the crystals is destroyed, which are of fundamental interest in surface sciences and help for a better understanding of the corresponding crystallization and melting in three-dimensional systems. On the other hand, the inherent polar layered ordering of the bent-core system resulting in (anti-)ferroelectricity and strongly intermolecular interaction suggests its potential for optoelectronic or other applications. For example, an all-organic ferroelectric field effect transistor has recently been brought forward,[40] where the gate insulator was made of ferroelectric films, displaying an enormous simplification of the production of technology compared to their inorganic counterparts and a wide space to enhance the device performance, implying forthcoming applications of banana-shaped compounds based on their ferroelectric, dielectric, and orientational properties. The clarity that AFM brings to the characterization, including film morphology, ordering, phase transition, and stability with temperature, of the vacuum-deposited films of the three-ring bent-core compound *m*-OSB will be valuable in efforts to produce the defect-free, highly oriented films of this class, and may provide us with possibilities of tailoring material structures to obtain suitable self-assembling and physical properties for such applications.

Acknowledgment. The work was financially supported by the Special Funds for Major State Basic Research Projects (2002CB613400) and the National Natural Science Foundation of China (90301008, 20025413).

References and Notes

(1) O'neill, M.; Kelly, S. M. *Adv. Mater.* **2003**, *13*, 1135, and references therein.

(2) Adam, D.; Schuhmacher, P.; Simmerer, J.; Häussling, L.; Siemnsmeyer, K.; Etzbach, K. H.; Ringsdorf, H.; Haarer, D. *Nature* **1994**, *371*, 141.

(3) Tokuhisa, H.; Era, M.; Tsutsui, T. *Adv. Mater.* **1998**, *10*, 404.

(4) Schmidt-Mende, L.; Fechtenkotter, A.; Müllen, K.; Moons, E.; Friend, R. H.; MacKenzie, J. D. *Science* **2001**, *293*, 1119.

(5) Van de Craats, A. M., Stutzmann, N.; Bunk, O.; Nielsen, M. M.; Watson, M.; Müllen, K.; Chanzy, H. D.; Sirringhaus, H.; Friend, R. H. *Adv. Mater.* **2003**, *15*, 495.

(6) Niori, T.; Sekine, F.; Watanabe, J.; Furukawa, T.; Takezoe, H. *J. Mater. Chem.* **1996**, *6*, 1231.

(7) Link, D. R.; Natale, G.; Shao, R.; Maclennan, J. E.; Clark, N. A.; Körblova, E.; Walba, D. M. *Science* **1997**, *278*, 1924.

(8) Thisayukta, J.; Nakayama, Y.; Kawauchi, S.; Takezoe, H.; Watanabe, J. *J. Am. Chem. Soc.* **2000**, *122*, 7441.

(9) Thisayukta, J.; Takezoe, H.; Watanabe, J. *Jpn. J. Appl. Phys.* **2001**, *40*, 3277.

(10) Macdonald, R.; Kentischer, F.; Warnick, P.; Heppke, G. *Phys. Rev. Lett.* **1998**, *81*, 4408.

(11) Shen, D.; Peganau, A.; Diele, S.; Wirth, I.; Tshierske, C. *J. Am. Chem. Soc.* **2000**, *122*, 1593.

(12) Dantlgraber, G.; Eremin, A.; Diele, S.; Hauser, A.; Kresse, H.; Pelzl, G.; Tchierske, C. *Angew. Chem., Int. Ed.* **2002**, *41*, 2408.

(13) Jákli, A.; Krüerke, D.; Sawade, H.; Chien, L. C.; Heppke, G. *Liq. Cryst.* **2002**, *29*, 377.

(14) Forrest, S. R. *Chem. Rev.* **1997**, *97*, 1793.

(15) Fraxedas, J. *Adv. Mater.* **2002**, *14*, 1603.

(16) Servet, B.; Horowitz, G.; Ries, S.; Lagorsse, O.; Alnot, P.; Yassar, A.; Deloffre, F.; Srivastava, P.; Hajlaoui, R.; Lang, P.; Garnier, F. *Chem. Mater.* **1994**, *6*, 1809.

(17) Zou, L.; Wang, J.; Beleva, V. J.; Kooijman, E. E.; Primak, S. V.; Risse, J.; Weissflog, W.; Jákli, A.; Mann, E. K. *Langmuir* **2004**, *20*, 2772.

(18) Kinoshita, Y.; Park, B.; Takezoe, H.; Niori, T.; Watanabe, J. *Langmuir* **1998**, *14*, 6256.

(19) Pelzl, G.; Diele, S.; Weissflog, W. *Adv. Mater.* **1999**, *11*, 707.

(20) Tang, Y. H.; Wang, Y.; Wang, X. D.; Wang, H. B.; Wang, L. X.; Yan, D. H. *J. Phys. Chem. B* **2004**, *108*, 12921.

(21) Walba, D. M.; Korblova, E.; Shao, R. F.; Maclenna, J. E.; Link, D. R.; Glaser, M. A.; Clark, N. A. *Science* **2000**, *288*, 2181.

(22) Watanaba, J.; Nakata, Y.; Simizu, K. *J. Phys. II (France)* **1994**, *4*, 581.

(23) Watanaba, J.; Niori, T.; Sekine, T.; Tekezoe, H. *Jpn. J. Appl. Phys.* **1998**, *37*, L139.

(24) Sarid, D. *Scanning Force Microscopy*; Oxford University Press: Oxford, 1991.

(25) Frommer, J. *Angew. Chem., Int. Ed. Engl.* **1992**, *31*, 1298.

(26) Boistelle, R.; Astier, J. P. *J. Crystal Growth* **1988**, *90*, 14.

(27) Mullin, J. W. *Crystallization*, 3rd ed.; Butterworth-Heinemann: Oxford, 1993.

(28) Liu, S. D.; Zhang, Z. Y.; Cosma, G.; Metiu, H. *Phys. Rev. Lett.* **1993**, *11*, 2967.

(29) Plass, K. E.; Kim, K.; Matzger, A. J. *J. Am. Chem. Soc.* **2004**, *126*, 9042.

(30) Dodabalapur, A.; Torsi, L.; Katz, H. E. *Science* **1995**, *268*, 270.

(31) Horowitz, G.; Hajlaoui, R.; Bouchriha, H.; Bourguiga, R.; Hajlaoui, M. *Adv. Mater.* **1998**, *10*, 923.

(32) Dinelli, F.; Murgia, M.; Levy, P.; Cavallini, M.; Biscarini, F.; Leeuw, D. M. D. *Phys. Rev. Lett.* **2004**, *92*, 116802.

(33) Lewis, B.; Campbell, D. S. *J. Vac. Sci. Technol.* **1967**, *4*, 209.

(34) Venables, J. A. *Philos. Mag.* **1973**, *27*, 697.

(35) Witten, T. A.; Sander, L. M. *Phys. Rev. Lett.* **1981**, *47*, 1400.

(36) Meakin, P. *Phys. Rev. A* **1983**, *27*, 1495.

(37) Zhang, Z. Y.; Chen, X.; Lagally, M. G. *Phys. Rev. Lett.* **1994**, *73*, 1829.

(38) Bales, C. S.; Chrzan, D. C. *Phys. Rev. Lett.* **1995**, *74*, 4879.

(39) Zhang, Z. Y.; Lagally, M. G. *Science* **1997**, *276*, 377.

(40) Schroeder, R.; Majewski, L. A.; Grell, M. *Adv. Mater.* **2004**, *16*, 633.